Imperial Journal of Interdisciplinary Research (IJIR)
Vol-3, Issue-10, 2017
ISSN: 2454-1362, http://www.onlinejournal.in

Modeling of Graphene Oxide Memory based on Hybridization State Modulation

Lim Ee Wah
Faculty of Electrical Engineering, Universiti Teknologi Malaysia, Skudai, Malaysia

***Abstract**: Graphene oxide (GO)-based resistive random access memory (RRAM) is one of the most promising emerging non-volatile memories for flexible electronics because of its simple structure and low fabrication cost. The reported switching mechanism can be classified into either localized or bulk effect. The localized effect is commonly observed in GO-RRAM with active electrode e.g. Cu and Al. The switching mechanism includes metallic conduction filament evolution or modification of interfacial resistance between GO layer and electrodes. On the other hand, the bulk effect involves hybridization state change of the entire GO layer and is typically observed in devices with inert electrode e.g. Pt and Au. Numerous compact models have been proposed for RRAM that are based on localized switching mechanism. However, compact modeling of GO-RRAM based on bulk mechanism is still lacking. Thus, this paper presents a compact model for GO-RRAM that relies on hybridization state modulation. The proposed model associates the resistance switching mechanism with the electrical-driven modification of sp^2 clusters density in the switching layer. A SPICE model incorporating the proposed compact model is developed for parameter calibration. The simulated I-V characteristic exhibits strong correlation with the experimental data. Hereby, we regard the proposed compact model as an acceptable and close description of GO-RRAM operation that depends on the bulk switching mechanism.*

1. Introduction

In view of various challenges in scaling floating-gate (FG) based memories beyond 10nm, research on the emerging non-volatile memory devices have gained substantial attention in recent years. Among the vastly studied technologies such as resistive random access memory (RRAM), spin-transfer torque magnetic RAM (STT-MRAM), ferroelectric RAM (FeRAM) etc., RRAM is regarded as one of the most popular memory technologies due to low fabrication cost, high performance and compatibility with conventional semiconductor process [1].

RRAM is usually a simple metal-insulator-metal (MIM) device. The resistance of its insulating layer is electrically tunable and thus suitable for use as a non-volatile memory device. Numerous materials have been found to demonstrate resistance switching phenomena, such as transition metal oxide (TMO), phase-change chalcogenides, organic materials, carbon-based materials and etc. [2-4]. Among these materials, graphene oxide (GO) is one of the most suitable materials for large area and flexible electronics [5]. GO films can be economically fabricated with the spin-coating method in room temperature [6].

To exploit the advantages of GO-RRAM in circuit design, a compact model with accurate I-V and SET/RESET characteristic is necessary. There are many compact models proposed for typical resistive switching memories, such as window-based [7-10], tunneling barrier model [11-13], equivalent circuit description [14-15], quantum point contact (QPC) model [16-17], phenomenological model [18] and filament evolution [19-21]. Some of these models are sufficient to describe the switching and transport operation of GO-RRAM that based on active electrode and metallic conductive filament (CF). However, compact modeling for GO-RRAM that based on transformation between sp^2 and sp^3 hybridization state is still lacking.

Therefore, we propose a compact model of the GO-RRAM device where the switching mechanism is associated with hybridization state modulation of the GO film. The model provides a compact description of both the switching and transport mechanism and a SPICE macro circuit that emblematizes the proposed compact model is developed to calibrate with experimental data and to facilitate circuit level simulation.

This article is organized as follows: the physical phenomenon of GO-based memristor operation is described in Section 2. The proposed compact model is outlined in Section 3. Circuit simulation and SPICE parameter calibration is reported in Section 4. Lastly, our conclusions are summarized.

2. Resistive Switching in Graphene Oxide Firm

GO film can be viewed as a stack of graphene sheets with intercalated oxygen functional groups (e.g. hydroxyl and epoxide) between basal planes. The bonds between carbon atoms and oxygen

functional groups are sp^3 hybridized, in contrast to the graphene-like sp^2 bonds between carbon atoms in basal planes. Figure 1 illustrates the simplified cross-sectional view of a multilayer graphene (MLG) and GO, respectively.

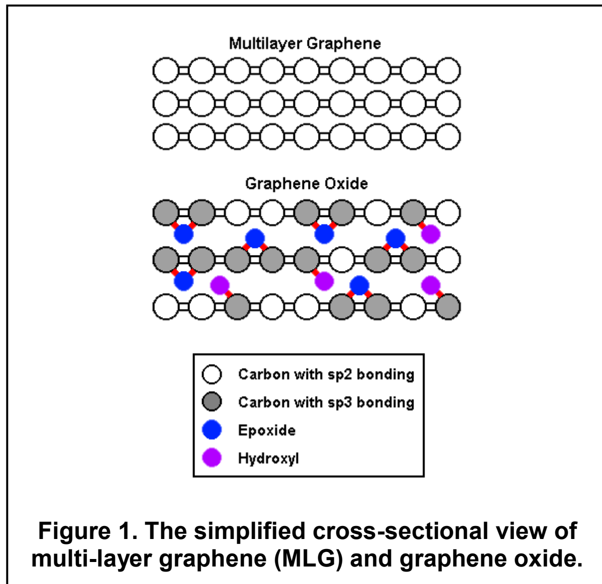

Figure 1. The simplified cross-sectional view of multi-layer graphene (MLG) and graphene oxide.

Resistive memories that use GO as the active layer have been reported in several works. Among these works, the switching mechanisms are typically associated with localized effects such as metallic CF evolution [23-24], resistance change in the interfacial oxide layer [25-27], or bulk effects such as hybridization state modulation of GO layers [28-30].

Switching mechanism of RRAM devices with chemically active electrodes (e.g. Cu) are often related to metallic CF formation and rupture process. These devices are also referred as electrochemical metallization memory (ECM) or conductive bridge RAM (CBRAM). In this case, the GO film does not play an active role in the resistive switching process and only acts as a solid electrolyte that accommodates the evolution of the metallic CF.

Another commonly reported localized effect is the reversible resistance change of the interfacial aluminum oxide (AlO_x) layer [6, 25-26]. This thin AlO_x layer is formed when the Al top electrode is deposited on the GO film during fabrication. Recently, the resistance switching phenomena within the AlO_x layer was experimentally proven to be related to the formation and rupture of CFs [26].

However, several works have indicated that the localized effect alone cannot explain the switching mechanism for all GO-RRAM devices. For example, the Pt/GO/ITO device reported by G.Khurana et al. [29] cannot be related to the interfacial mechanism because an inert electrode is used. Additionally, the device has an initial state at low resistance state (LRS), which limits the possibility of filamentary mechanism. S.Porro et al. [30] confirmed the absence of an interfacial oxide layer and metal filament in the reported Ag/GO/ITO sample based on XPS depth analysis. Thus, in addition to the localized effect, the hybridization change in the GO film could be a governing switching mechanism for some GO-RRAM devices. The correlation between the conductivity of GO and sp^2 density have been demonstrated experimentally in several works [29], [31]. Hence, in this work, a compact model for GO-RRAM devices that is dominated by bulk mechanism is proposed.

Pristine GO film has a high density of sp^3-bonded structures due to the presence of intercalated oxygen functional groups. Depending on the oxidation level, there is a small number of sp^2 clusters distributed across the GO film. As shown in Figure 2, these graphene-like clusters are isolated by the amorphous sp^3 matrix, which introduces high tunneling barrier and substantially limits the electrons tunneling probability between the sp^2 clusters. The initial resistance state can be either LRS [29] or high resistance state (HRS) [30] depending on the initial density of the sp^2 clusters. During the SET operation, sp^2 density is increased by electrically reduction of oxygen functional groups. The increasing number of sp^2 cluster induces additional vertically aligned hopping paths for the electrons and thus switches the device into LRS [32] as shown in Figure 2(b).

On the other hand, during the RESET operation, the positive voltage is applied to the top electrode. Oxygen ions migrate back into the GO layer and hybridize the sp^2 clusters back into high resistance sp^3 bonding. This effectively reduces the sp^2 density, breaks the hopping chain and switches the device back into HRS.

3. Compact Modeling Description

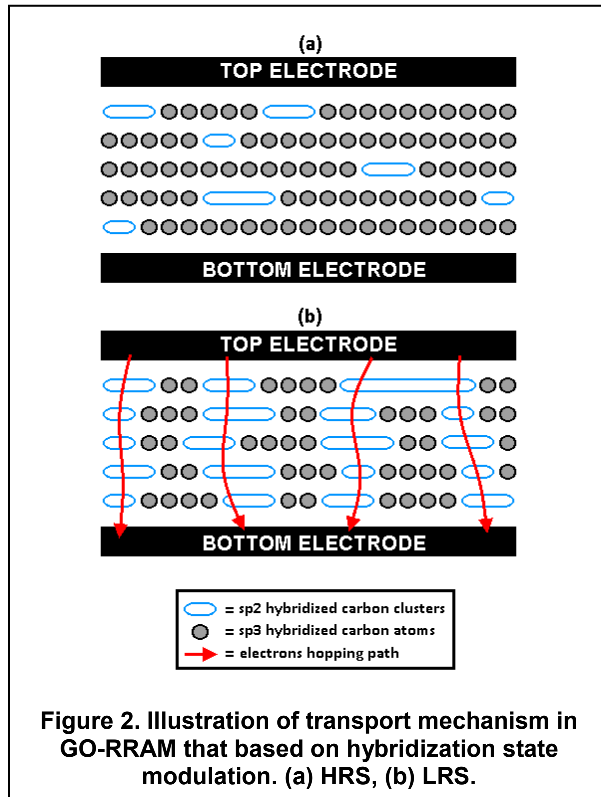

Figure 2. Illustration of transport mechanism in GO-RRAM that based on hybridization state modulation. (a) HRS, (b) LRS.

Electron transportation over the percolating sp^2 clusters can be modeled with multi-phonon trap-assisted tunneling (MTAT) mechanism [32]. The sp^2 clusters act as intermediate traps supporting continuous electron flow. The steady state current is always limited by the slowest trap due to conservation of the electric charge.

For simplicity, this compact model assumes equal interlayer distance and voltage drop across the traps. Thus, the resulting current over a single chain can be expressed in the form of Eq. (1) [33-34] as in Figure 2, which q is elementary charge; τ_c and τ_e are the time constants for capture and emission rate of a trap. The time constants are correlated with the capture/emission rate of the trap and tunneling probability (P_T). The capture and emission rate are estimated using 3D delta potential of the traps [35] and have a square function of applied field [32].

One the other hand, the tunneling probability is estimated using Wentzel-Kramers-Brillouin (WKB) approximation and can be written as Eq. (2) [36], which $m*$ is the electron effective mass; $\hbar$ is Planck's constant; E_T represents the trap energy; F is the electrical field and d represents the interlayer distance. Thus, the current flow over a percolating chain of sp^2 clusters can be generalized to Eq. (3), where K_{path} is the physical parameter obtained from numerical simulation as reported in [32]. N is the state variable representing number of conducting path.

The resistance state of GO-RRAM can be modulated by controlling the sp^2 concentration of GO film. In this model, the sp^2 density change is related to the redox rate of the intercalated oxygen functional groups. The SET process involves reduction of oxygen function groups and breaking of the sp^3 bonds. The probability of the process can be expressed with Boltzmann distribution as Eq. (5) [37], where v_0 is the thermal vibration frequency of the oxygen function groups. E_a is the zero-field effective activation energy required to break the sp^3 bonds. ΔE represents the field-induced energy barrier lowering.

$$I_{path} = q \cdot \frac{1}{\tau_c + \tau_e} \tag{1}$$

$$P_T = exp\left[-\frac{4}{3\hbar qF}\sqrt{2m^*}\left({E_T}^{3/2} - (E_T - qFd)^{3/2}\right)\right] \tag{2}$$

$$I_{path} = K_{path}F^2 exp\left[-\frac{4\sqrt{2m^*}}{3\hbar} \cdot \frac{\left({E_T}^{3/2} - (E_T - qFd)^{3/2}\right)}{qF}\right] \tag{3}$$

$$I = N \cdot I_{path} \tag{4}$$

$$P_G = v_0 \cdot exp\left(-\frac{E_a - \Delta E}{kT}\right) \tag{5}$$

$$P_R = \beta_R \cdot v_0 \cdot exp\left(-\frac{E_m}{kT}\right) \tag{6}$$

$$\beta_R = \beta_0 exp[k_0(V - V_0)] \tag{7}$$

$$\frac{dN}{dt} \propto v_0\left[exp\left(-\frac{E_a - V \cdot d/L}{kT}\right) - \beta_0 exp(k(V - V_0))exp\left(-\frac{E_m}{kT}\right)\right] \tag{8}$$

$$E_a = E_{a(min)} + \left(E_{a(max)} - E_{a(min)}\right)exp\,(-\alpha V) \tag{9}$$

$$T = T_0 + V \cdot I \cdot R_{th} \tag{10}$$

Figure 3. Compact Modeling Equations.

The RESET process involves recombination of the oxygen function groups back to the graphene basal plane. This process essentially turns the sp^2 clusters back into sp^3 bonds. The recombination rate has a strong correlation with the capture region of sp^2 cluster. When a high electric field is applied, the electron occupation rate at the sp^2 clusters will be lowered significantly. This will increase the capture region of sp^2 clusters and thus increase the recombination rate of the oxygen function groups [37].

The recombination rate can be written as in Eq. (6), where E_m is the oxygen migration barrier and β_R represents the enhancement factor of the recombination rate due to increased capture region of the vacancy. β_R is voltage dependent and can be expressed as Eq. (7) [38] where β_0 represents the recombination rate multiplier at zero biased; V_0 is the threshold voltage in which all electrons in the vacancies are fully depleted; k_0 represents the multiplication factor. By combining Eq. (4), (5) and (6), the sp^2 concentration change rate can be expressed in a compact form as in Eq. (8), where N is the number of percolating conducting path, which

correlates to the *sp*^{2} concentration. E_a and E_m are the activation and migration energy of the oxygen functional groups. The voltage polarity of the generation rate (P_G) is inverted because the SET operation happens in the negative region. It worth noting that the SET operation is several orders faster than the RESET operation in GO-RRAM.

During the SET operation (negative bias), electrons are injected from the top electrode and this increases the electron density in GO layer. According to the density functional theory (DFT) calculation, the energy barrier may reduce from 0.73eV in neutral GO down to 0.15eV when electron density is increased [39]. The effective energy barrier lowering at SET operation is modeled as exponential decay function of applied voltage as in Eq. (9), where α is a fitting parameter representing the barrier reduction rate versus applied voltage. E_a(min) and E_a(max) are 0.15eV and 0.73eV respectively [39].

In addition to the transport and switching modeling, thermal effect has to be considered as well. In this proposed model, a simplified equation is applied to describe the Joule heating effect. The average device temperature is modeled with an effective thermal resistance as shown in Eq. (10) [40], where I represents the current flowing through the device and R_{th} is the equivalent thermal resistance of the GO-RRAM device which has a unit of K/W.

4. Electrical Circuit Modeling and Simulation

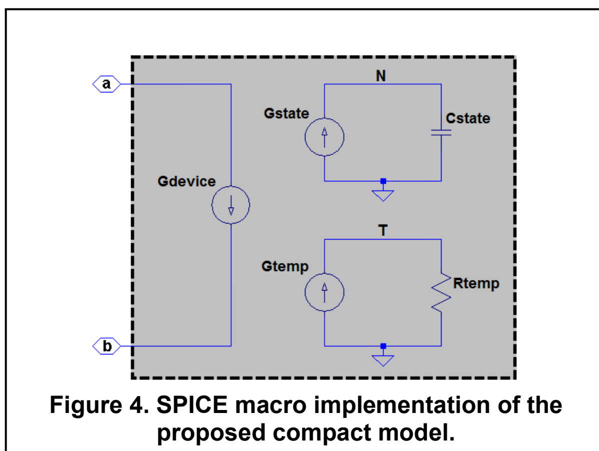

Figure 4. SPICE macro implementation of the proposed compact model.

A SPICE macro is developed for parameter calibration and model validation. Figure 4 depicts the SPICE implementation of the GO-RRAM macro. The G_{device} current source models the current flow between the electrodes based on the transport equations stated in Eq. (5). The voltage at N node serves as a state variable emulating *sp*^{2} cluster density of the GO-RRAM device. The G_{state} current source modifies the stored charges at C_{state} capacitor according to the *sp*^{2} concentration change rate stated in Eq. (9). Temperature evolution of the device is modeled as voltage at T node. R_{temp} represents the equivalent thermal resistance of the GO-RRAM.

The SPICE parameter is calibrated with the Pt/GO/ITO RRAM device reported in [29]. The GO active layer is 30*nm* in thickness and is deposited on the ITO coated glass using the spin-coating method. The electrical measurements were done in room temperature. The calibrated parameters is shown in Table 1.

Table 1. Table example.

Parameters	*Value*	*Unit*
I_{cc}	*32*	*mA*
K_{path}	1.22×10^{-5}	AV^{-2}
A_{cell}	1.26×10^{-9}	m^2
S_{LRS}	5.79×10^{12}	m^{-2}
S_{HRS}	1.29×10^{10}	m^{-2}
A_{PT}	*-24.7*	$VJ^{-3/2}$
E_T	*4.5*	*eV*
E_a	*0.15 - 0.73*	*eV*
α	*0.25*	-
E_m	*0.62*	*eV*
β_0	*1*	-
k_0	*100*	-
V_0	*3.2*	*V*
v_0	10^{13}	*Hz*
R_{th}	*200*	*W/K*
T_0	*300*	*K*
d	*1*	*nm*
L	*30*	*nm*

The I_{cc} represents the compliance current. K_{path} is a physical parameter used in Eq. (3). A_{cell} is the active device area that participates in the resistive switching process. S_{LRS} and S_{HRS} represent the density of percolating current paths in LRS and HRS, respectively. Total conducting paths in the cell can be obtained by normalized to the effective device area, e.g. $N_{LRS} = S_{LRS} \times A_{cell}$. A_{PT} is a generalized physical parameters used in Eq. (2). E_T is the trap energy in the GO film [41]. Parameters E_a and E_m are the oxygen migration barriers during SET and RESET operation, respectively. α is fitting parameter representing the reduction rate of the activation energy when electron density increase. β_0, k_0 and V_0 are parameters describing the enhancement factor of the recombination rate as in Eq. (7). v_0 is the thermal vibration frequency of the oxygen ions. R_{th} is the equivalent thermal resistance. T_0, d and L are room temperature, interlayer distance of graphene sheet and device thickness, respectively.

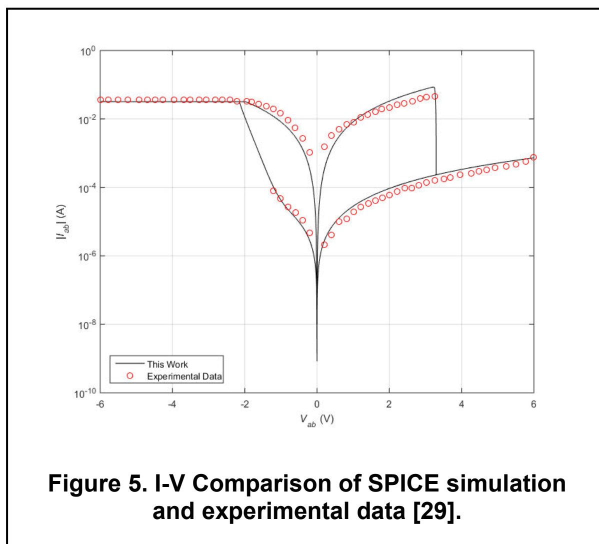

Figure 5. I-V Comparison of SPICE simulation and experimental data [29].

The voltage stimulus is a triangular waveform with amplitude of 6V and ramp rate of 40V/s. The resulting current flow is plotted in a semi-logarithmic plot as shown in Figure 5. The simulated I-V characteristic demonstrates a good correlation with the experimental data.

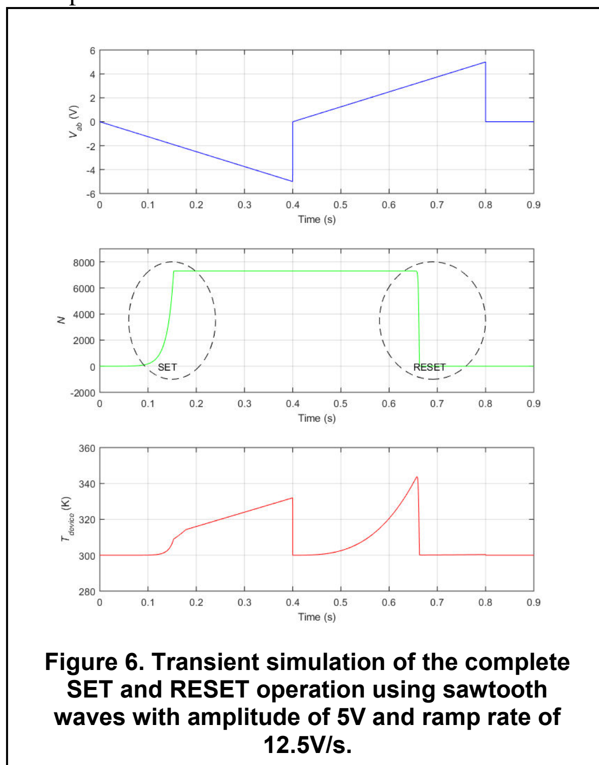

Figure 6. Transient simulation of the complete SET and RESET operation using sawtooth waves with amplitude of 5V and ramp rate of 12.5V/s.

Figure 6 illustrates the evolution of the number of current path (*N*) and the average device temperature (T_{device}) when the input voltage is ramped from zero to -5V (SET) and then to 5V (RESET). During the SET operation, the density of the sp^2 cluster is gradually built up when the voltage ramps toward the negative regime. During the RESET operation, the sp^2 density drops when the device is positively biased by more than 3.2 V. It is worth noting that the SET operation started at a much lower voltage than the RESET operation. This apparent difference can be explained by the lower oxygen migration barrier being induced by the increased electron density at the GO layer when the electrons are injected from the top electrode during SET operation [39].

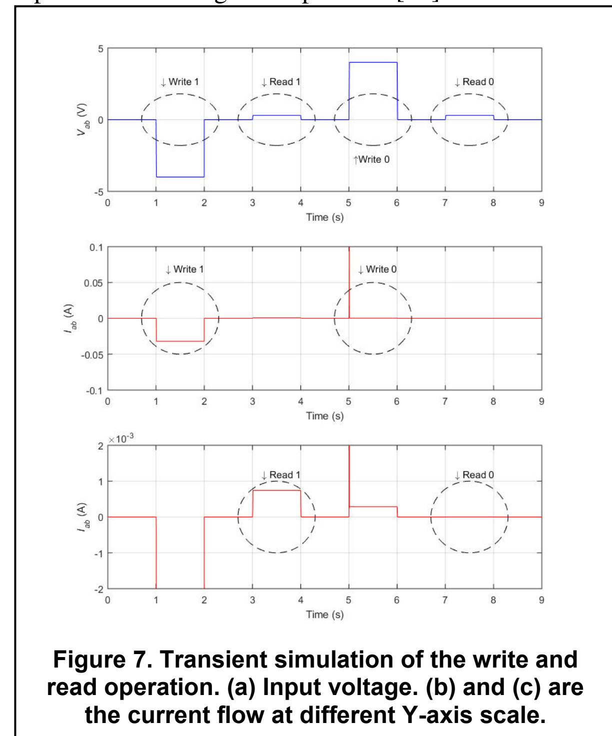

Figure 7. Transient simulation of the write and read operation. (a) Input voltage. (b) and (c) are the current flow at different Y-axis scale.

Figure 7 shows the transient response of the SPICE macro for a sequence of write-1, read-1, write-0 and then read-0 operations. The write pulse is set to 4V with a pulse width of one second. The read operations are carried out by applying a low-voltage (0.3V). The effective resistance of LRS and HRS are 405Ω and 184kΩ, respectively. This implies a LRS/HRS ratio of 450 for this Pt/GO/ITO sample.

5. Conclusion

In summary, a compact modeling for GO-RRAM has been presented. The charge transport mechanism is associated with MTAT mechanism, in which the electrons tunnel through GO layers assisted by the vertically aligned sp^2 clusters. Resistance state of the device is associated with the sp^2 clusters density. The SET operation increases sp^2 cluster density through electrically induced reduction of oxygen functional groups. Meanwhile, the RESET operation is associated with oxygen ion migration and re-hybridization of the sp^2 clusters. The IV characteristic of the proposed compact model has high correlation with the experimental data. Circuit operations such as read and write are simulated and analyzed in transient mode. Therefore, the proposed model is regarded as a compact, and yet an accurate description for circuit level simulation.

6. Acknowledgements

The author would like to thank Ministry of Education Malaysia of the MyBrain15 scholarship and Research Management Centre (RMC) of Universiti Teknologi Malaysia (UTM) for providing an excellent research environment in which to complete this work

7. References

[1] J. S. Meena, S. M. Sze, U. Chand, and T.-Y. Tseng, "Overview of emerging nonvolatile memory technologies.," *Nanoscale Res. Lett.*, vol. 9, no. 1, p. 526, 2014.

[2] M. Lanza, "A review on resistive switching in high-k dielectrics: A nanoscale point of view using conductive atomic force microscope," *Materials (Basel).*, vol. 7, no. 3, pp. 2155–2182, 2014.

[3] M. Ghoneim and M. Hussain, "Review on Physically Flexible Nonvolatile Memory for Internet of Everything Electronics," *Electronics*, vol. 4, no. 3, pp. 424–479, 2015.

[4] S. Porro, E. Accornero, C. F. Pirri, and C. Ricciardi, "Memristive devices based on graphene oxide," *Carbon N. Y.*, vol. 85, pp. 383–396, 2015.

[5] J. Liu, Z. Yin, X. Cao, F. Zhao, L. Wang, W. Huang, and H. Zhang, "Fabrication of flexible, all-reduced graphene oxide non-volatile memory devices," *Adv. Mater.*, vol. 25, no. 2, pp. 233–238, 2013.

[6] H. Y. Jeong, J. Y. Kim, J. W. Kim, J. O. Hwang, J. E. Kim, J. Y. Lee, T. H. Yoon, B. J. Cho, S. O. Kim, R. S. Ruoff, and S. Y. Choi, "Graphene oxide thin films for flexible nonvolatile memory applications," *Nano Lett.*, vol. 10, no. 11, pp. 4381–4386, 2010.

[7] D. B. Strukov, G. S. Snider, D. R. Stewart, and R. S. Williams, "The missing memristor found," *Nature*, vol. 453, no. 7191, pp. 80–3, 2008.

[8] Z. Biolek, D. Biolek, and V. Biolková, "SPICE model of memristor with nonlinear dopant drift," *Radioengineering*, vol. 18, no. 2, pp. 210–214, 2009.

[9] Y. N. Joglekar and S. J. Wolf, "The elusive memristor: properties of basic electrical circuits," *Eur. J. Phys.*, vol. 30, no. 4, p. 661, 2009.

[10] T. Prodromakis, B. P. Peh, C. Papavassiliou, and C. Toumazou, "A versatile memristor model with nonlinear dopant kinetics," *IEEE Trans. Electron Devices*, vol. 58, no. 9, pp. 3099–3105, 2011.

[11] M. D. Pickett, D. B. Strukov, J. L. Borghetti, J. J. Yang, G. S. Snider, D. R. Stewart, and R. S. Williams, "Switching dynamics in titanium dioxide memristive devices," *J. Appl. Phys.*, vol. 106, no. 7, pp. 1–6, 2009.

[12] S. Kvatinsky, E. G. Friedman, A. Kolodny, and U. C. Weiser, "TEAM: Threshold adaptive memristor model," *IEEE Trans. Circuits Syst. I Regul. Pap.*, vol. 60, no. 1, pp. 211–221, 2013.

[13] I. Vourkas and G. C. Sirakoulis, *Memristor-Based Nanoelectronic Computing Circuits and Architectures*. Springer International Publishing, 2016.

[14] J. Blasco, N. Ghenzi, J. Suñé, P. Levy, and E. Miranda, "Equivalent circuit modeling of the bistable conduction characteristics in electroformed thin dielectric films," *Microelectron. Reliab.*, vol. 55, no. 1, pp. 1–14, 2015.

[15] J. H. Hur, M. J. Lee, C. B. Lee, Y. B. Kim, and C. J. Kim, "Modeling for bipolar resistive memory switching in transition-metal oxides," *Phys. Rev. B - Condens. Matter Mater. Phys.*, vol. 82, no. 15, pp. 1–5, 2010.

[16] E. A. Miranda, C. Walczyk, C. Wenger, and T. Schroeder, "Model for the Resistive Switching Effect in HfO2 MIM Structures Based on the Transmission Properties of Narrow Constrictions," *IEEE Electron Device Lett.*, vol. 31, no. 6, pp. 609–611, 2010.

[17] R. Degraeve, A. Fantini, N. Raghavan, L. Goux, S. Clima, Y. Y. Chen, A. Belmonte, S. Cosemans, D. J. Wouters, P. Roussel, G. S. Kar, G. Groeseneken, and M. Jurczak, "Hourglass concept for RRAM : a dynamic and statistical device model," in *International Symposium on the Physical and Failure Analysis of Integrated Circuits (IPFA)*, 2014, no. 2, pp. 245–249.

[18] F. Merrikh Bayat, B. Hoskins, and D. B. Strukov, "Phenomenological modeling of memristive devices," *Appl. Phys. A Mater. Sci. Process.*, vol. 118, no. 3, pp. 779–786, 2015.

[19] X. Guan, S. Yu, and H. S. P. Wong, "A SPICE compact model of metal oxide resistive switching memory with variations," *IEEE Electron Device Lett.*, vol. 33, no. 10, pp. 1405–1407, 2012.

[20] S. Menzel, U. Böttger, and R. Waser, "Simulation of multilevel switching in electrochemical metallization memory cells," in *Journal of Applied Physics*, vol. 111, no. 1, A. Chan, Ed. 2012, pp. 6–11.

[21] H. Li, P. Huang, B. Gao, B. Chen, X. Liu, and J. Kang, "A SPICE model of resistive random access memory for large-scale memory array simulation," *IEEE Electron Device Lett.*, vol. 35, no. 2, pp. 211–213, 2014.

[22] H. He, J. Klinowski, M. Forster, and A. Lerf, "A new structural model for graphite oxide," *Chem. Phys. Lett.*, vol. 287, no. 1–2, pp. 53–56, 1998.

[23] F. Zhuge, B. Hu, C. He, X. Zhou, Z. Liu, and R. W. Li, "Mechanism of nonvolatile resistive switching in graphene oxide thin films," *Carbon N. Y.*, vol. 49, no. 12, pp. 3796–3802, 2011.

[24] C. L. He, F. Zhuge, X. F. Zhou, M. Li, G. C. Zhou, Y. W. Liu, J. Z. Wang, B. Chen, W. J. Su, Z. P. Liu, Y. H. Wu, P. Cui, and R. W. Li, "Nonvolatile resistive switching in graphene oxide thin films," *Appl. Phys. Lett.*, vol. 95, no. 23, pp. 2013–2016, 2009.

[25] H. W. Nho, J. Y. Kim, J. Wang, H. J. Shin, S. Y. Choi, and T. H. Yoon, "Scanning transmission X-ray microscopy probe for in situ mechanism study of graphene-oxide-based resistive random access memory," *J. Synchrotron Radiat.*, vol. 21, no. 1, pp. 170–176, 2014.

[26] S. K. Kim, J. Y. Kim, S. Y. Choi, J. Y. Lee, and H. Y. Jeong, "Direct Observation of Conducting Nanofilaments in Graphene-Oxide-Resistive Switching Memory," *Adv.*

Funct. Mater., pp. 6710–6715, 2015.

[27] S. K. Pradhan, B. Xiao, S. Mishra, A. Killam, and A. K. Pradhan, "Resistive switching behavior of reduced graphene oxide memory cells for low power nonvolatile device application," *Sci. Rep.*, vol. 6, no. April, p. 26763, 2016.

[28] L. H. Wang, W. Yang, Q. Q. Sun, P. Zhou, H. L. Lu, S. J. Ding, and D. Wei Zhang, "The mechanism of the asymmetric SET and RESET speed of graphene oxide based flexible resistive switching memories," *Appl. Phys. Lett.*, vol. 100, no. 6, pp. 3–7, 2012.

[29] G. Khurana, P. Misra, and R. S. Katiyar, "Forming free resistive switching in graphene oxide thin film for thermally stable nonvolatile memory applications," *J. Appl. Phys.*, vol. 114, no. 12, 2013.

[30] S. Porro and C. Ricciardi, "Memristive behaviour in inkjet printed graphene oxide thin layers," *RSC Adv.*, vol. 5, pp. 68565–68570, 2015.

[31] V. Rai, M. K. Kavitha, and M. Jaiswal, "Correlating Chemical Structure and Charge Transport in Reduced Graphene Oxide for Transparent Conductor and Interconnect Applications," *2015 IEEE Int. Symp. Nanoelectron. Inf. Syst.*, pp. 164–169, 2015.

[32] E. W. Lim, M. T. Ahmadi, and R. Ismail, "Modeling and simulation of graphene-oxide-based RRAM," *J. Comput. Electron.*, vol. 15, no. 2, pp. 602–610, 2016.

[33] F. Schuler, R. Degraeve, P. Hendrickx, and D. Wellekens, "Physical description of anomalous charge loss in floating gate based NVM's and identification of its dominant parameter," *2002 IEEE Int. Reliab. Phys. Symp. Proceedings. 40th Annu. (Cat. No.02CH37320)*, pp. 26–33, 2002.

[34] G. Bersuker, J. Yum, L. Vandelli, a. Padovani, L. Larcher, V. Iglesias, M. Porti, M. Nafría, K. McKenna, a. Shluger, P. Kirsch, and R. Jammy, "Grain boundary-driven leakage path formation in HfO2 dielectrics," *Solid. State. Electron.*, vol. 65–66, no. 1, pp. 146–150, 2011.

[35] M. Herrmann and a. Schenk, "Field and high-temperature dependence of the long term charge loss in erasable programmable read only memories: Measurements and modeling," *J. Appl. Phys.*, vol. 77, no. 9, pp. 4522–4540, 1995.

[36] M. P. Houng, Y. H. Wang, and W. J. Chang, "Current transport mechanism in trapped oxides: A generalized trap-assisted tunneling model," *J. Appl. Phys.*, vol. 86, no. 3, p. 1488, 1999.

[37] X. Guan, S. Yu, and H. S. P. Wong, "On the switching parameter variation of metal-oxide RRAM - Part I: Physical modeling and simulation methodology," *IEEE Trans. Electron Devices*, vol. 59, no. 4, pp. 1172–1182, 2012.

[38] Y. Lu, B. Gao, Y. H. Fu, B. Chen, L. F. Liu, X. Y. Liu, and J. F. Kang, "A Simplified Model for Resistive Switching of Oxide-Based Resistive Random Access Memory Devices," *Ieee Electron Device Lett.*, vol. 33, no. 3, pp. 306–308, 2012.

[39] A. M. Suarez, L. R. Radovic, E. Bar-Ziv, and J. O. Sofo, "Gate-Voltage Control of Oxygen Diffusion on Graphene," *Phys. Rev. Lett.*, vol. 106, no. 14, p. 146802, Apr. 2011.

[40] Z. Jiang, S. Yu, Y. Wu, J. H. Engel, X. Guan, and H. S. P. Wong, "Verilog-A Compact Model for Oxide-based Resistive Random Access Memory (RRAM)," *IEEE*, no. 2, pp. 41–44, 2014.

[41] J. H. Kim, J. H. Hwang, J. Suh, S. Tongay, S. Kwon, C. C. Hwang, J. Wu, and J. Young Park, "Work function engineering of single layer graphene by irradiation-induced defects," *Appl. Phys. Lett.*, vol. 103, no. 17, 2013.